Published in final edited form as:
Biochemistry. 2012 November 6; 51(44): 9014–9026. doi:10.1021/bi301103j.

Denaturation of RNA secondary and tertiary structure by urea: simple unfolded state models and free energy parameters account for measured *m*-values

Dominic Lambert[†] and **David E. Draper**[*]
Department of Chemistry, Johns Hopkins University, Baltimore, MD 21218

Abstract

To investigate the mechanism by which urea destabilizes RNA structure, urea-induced unfolding of four different RNA secondary and tertiary structures was quantified in terms of an *m*-value, the rate at which the free energy of unfolding changes with urea molality. From literature data and our osmometric study of a backbone analog, we derived average interaction potentials (per $Å^2$ of solvent accessible surface) between urea and three kinds of RNA surfaces: phosphate, ribose, and base. Estimates of the increases in solvent accessible surface areas upon RNA denaturation were based on a simple model of unfolded RNA as a combination of helical and single strand segments. These estimates, combined with the three interaction potentials and a term to account for urea interactions with released ions, yield calculated *m*-values in good agreement with experimental values (200 m*m* monovalent salt). Agreement was obtained only if single-stranded RNAs were modeled in a highly stacked, A form conformation. The primary driving force for urea induced denaturation is the strong interaction of urea with the large surface areas of bases that become exposed upon denaturation of either RNA secondary or tertiary structure, though urea interactions with backbone and released ions may account for up to a third of the *m*-value. Urea *m*-values for all four RNA are salt-dependent, which we attribute to an increased extension (or decreased charge density) of unfolded RNAs with increased urea concentration. The sensitivity of the urea *m*-value to base surface exposure makes it a potentially useful probe of the conformations of RNA unfolded states.

Introduction

An important component of the free energy of macromolecule denaturation derives from solvent interactions with newly exposed surfaces of the unfolded molecules. Various solvent additives (co-solvents) may alter the balance of favorable and unfavorable interactions at exposed surfaces and stabilize either the native or denatured conformation. In fact, urea-induced denaturation of proteins has long been used as a way to gain insights into the origins of protein stability (3, 4). Particularly remarkable was the observation that the urea-dependence of the unfolding free energy (the so-called *m*-value) is proportional to the increase in solvent-accessible surface area (SASA) that accompanies protein unfolding (5). Further studies have found quantitative relationships between urea interactions with model compounds, protein surface areas exposed upon denaturation, and the urea-dependence of protein unfolding free energy (6-10).

[*]Corresponding author: Tel 410 516 7448. Fax 410 516 8420. draper@jhu.edu. .
[†]Present address: Bureau of Microbial Hazards, HPFB, Health Canada, 251 Sir Frederick Banting Driveway, PL2204E, Ottawa, Ontario, Canada, K1A 0K9

Urea also denatures both RNA secondary and tertiary structures and could potentially provide a tool for assessing the extent to which different RNA surfaces are exposed upon denaturation. Urea strongly solubilizes nucleic acid bases (11), which is presumably a major factor driving the denaturation of nucleic acid secondary structure. RNA tertiary structures may include extensive hydrogen bonding of both ribose and phosphate, and thus might be expected to respond differently to urea than RNA secondary structures. At present, few studies have attempted to quantify the urea-dependence of unfolding different types of RNA structure or provide a quantitative model of the denaturation mechanism (12-14).

In a previous study, we quantified the stabilization of RNA tertiary structures by the protecting osmolyte trimethylamine oxide (TMAO), and concluded that TMAO promotes compact RNA conformations primarily because of its exclusion from the strongly hydrated anionic oxygens of phosphate (15). In this study, our purpose is to provide similar measurements of *m*-values for urea induced unfolding of RNA tertiary structures and to identify the main urea – RNA interactions that cause denaturation. We devise a simple model of the RNA unfolded state that, used in conjunction with a set of four "interaction potentials" based on urea interactions with KCl and model compounds, quantitatively accounts for the observed urea-dependence of the unfolding free energies. The *m*-values for urea and RNA are dominated by favorable interactions of urea with base surfaces exposed upon denaturation. Urea and TMAO are thus complementary probes of the changes in solvent accessibility that accompany RNA conformational transitions, one reporting primarily on base surfaces and the other on backbone phosphates.

Materials & Methods

Chemicals and solutions

All solutions were prepared using distilled deionized water at 18.3MΩ resistivity. MOPS, potassium chloride, and urea (all >99.5% pure) were purchased from Fluka; potassium hydroxide was from Aldrich. TMAO was purchased from Fluka and purified as described (15). The synthesis and preparation of dry potassium dimethylphosphate was as described (15).

Poly(A) was purchased from CalBiochem. The hairpin, tar, and tar* RNAs were purchased from Dharmacon and deprotected according the manufacturer's directions. The other RNAs (TLR and A-riboswitch) were prepared by *in vitro* transcription with T7 RNA polymerase from linearized plasmid DNA and purified by denaturing polyacrylamide gel electrophoresis followed by electroelution, as described (14).

UV- and CD-monitored unfolding of RNAs

For melting and CD experiments, RNAs were extensively equilibrated with the appropriate buffers, using Amicon Ultra centrifugal filter devices. KMOPS buffer contained 10 mmolal MOPS (adjusted to pH 7.0 with 4 m*m* KOH) and 2 Omolal EDTA (20 μM for CD titrations) in addition to the desired concentrations of KCl and urea. Experiments with the A riboswitch RNA contained 2,6 diaminopurine (DAP) as ligand, concentrations were 5 μ*m* for melting experiments and 100 μ*m* for CD titrations. Osmolyte solutions were prepared gravimetrically from stock solutions of known density.

Thermal denaturation of the RNAs was monitored by absorbance in a Cary 400 spectrophotometer with a six cell, temperature-controlled cuvette holder. Data were collected at 260 and 280 nm between 5 and 95 °C. A programmed series of heating and cooling steps was designed to insure renaturation of the RNA and to check for hysteresis below 65 °C (16). For the hairpin RNA, absorbance vs. temperature curves were analyzed in the usual way to obtain $\Delta H°$ and T_m, with allowance for sloping baselines at low and high

temperatures (17). Data for the other RNAs studied were plotted as the first derivative of absorbance with respect to temperature and fit to sequential two-state transitions defined by T_m, $\Delta H°$ and amplitude of absorbance change. Both the 260 and 280 nm data were fit to the same T_m and $\Delta H°$ parameters by a global fitting program, which also calculated parameter errors by bootstrap analysis (18). Free energy of unfolding, ΔG°_{unfold}, was calculated at 25 °C by $\Delta G^\circ_{unfold}=\Delta H^\circ (T_0/T_m - 1)$ where T_0 is 298 K.

Titrations of the A riboswitch with urea were performed at 15 °C with an Aviv Model 400 CD Spectrometer equipped with a Hamilton Microlab 500 automated titrator. The initial buffer (10 m*m* KMOPS, 100 m*m* KCl, 20 μ*m* EDTA, 100 μ*m* DAP) was titrated with the same buffer also containing 9 *m* urea. Titration data were fit to an equation with six variables specifying the slopes and intercepts of baselines for the unfolded and folded RNAs and a urea-dependent equilibrium constant expressed in terms of the midpoint of the titration and the *m*-value.

Analysis of the salt dependence of RNA stability

The negative charge of an RNA in a KCl buffer is neutralized by an overall excess of K^+ and a deficiency of Cl^-, relative to the concentrations of the ions at a distance from the RNA. The thermodynamic parameter Γ_+ can be considered the fraction of polynucleotide phosphate charges neutralized by excess cations; the similar parameter that reflects the deficiency of anions, Γ_-, is negative (19). Because charge neutrality is maintained in a solution, $\Gamma_+ - \Gamma_- = 1$. Upon unfolding, there is a decrease in the number of excess cations, $\Delta\Gamma_+$, matched by a equivalent decrease in Γ_- to a more negative value. The preceding relation between Γ_+ and Γ_- requires $\Delta\Gamma_+ = \Delta\Gamma_-$; we call either of these quantities $\Delta\Gamma_\pm$. Thus, there is a net release of $\Delta\Gamma_\pm$ ion pairs (K^+ and Cl^-) or $2\Delta\Gamma_\pm$ total ions (20, 21). $\Delta\Gamma_\pm$ is experimentally derived from the salt-dependence of the RNA stability by the Wyman linkage relation

$$-\left(\frac{1}{RT}\right)\left(\frac{\partial \Delta G^o_{obs}}{\partial \ln a_\pm}\right)=2\Delta\Gamma_\pm \quad (1)$$

where ΔG°_{obs} is the free energy of RNA unfolding obtained from the mole ratio of unfolded to folded RNA, $a_\pm$ is the mean ionic activity, R is the gas constant, and T the temperature. ΔG°_{obs} for unfolding an RNA at various KCl concentrations was derived from melting experiments as described above. $2\Delta\Gamma_\pm$ was obtained from linear fits of ΔG°_{obs} *vs.* $\ln(m_{K+})$, after correction of the slope for the concentration dependence of the KCl mean ion activity coefficient, as described (21).

VPO and μ_{23} calculations

A Westcor VAPRO 5520 (Logan, UT) was used for vapor pressure osmometry as described (15). The instrument is designed to calibrate with standards provided by the manufacturer, at 100, 290, and 1000 mOsm (milli osmolality). In addition to this calibration, KCl standards were prepared gravimetrically to give readings in the range of 800 – 2000 mOsm; osmolality was calculated from molality by the Pitzer equation (22). These standards were read alternately with KDMP to yield a calibration curve for higher osmolalities.

Poly(A) was dissolved in 50 mm MOPS buffer (adjusted to pH 7.0 with KOH) and dialyzed extensively against the same buffer before use. The poly(A) concentration was determined by UV absorbance after base hydrolysis. Solutions were assembled gravimetrically from stocks of known molality or density. Triplicate readings were made on each sample. For

poly(A) samples, urea or TMAO was a constant 1 *m*; KDMP samples contained a range of urea from 0.757 to 0.899 *m*.

The reading reported by the VPO instrument is the solution osmolality, which is

$$\mathrm{Osm} \equiv -m^{\bullet}_{\mathrm{water}} \ln a_{\mathrm{water}} \quad (2)$$

where $m^{\bullet}_{\mathrm{water}} \equiv 55.5$ mol/kg, the molality of water, and a_{water} is the measured thermodynamic activity of water in the solution. To calculate μ_{23}, a chemical potential derivative that quantifies interactions between two solutes (see Results, eq 6), we find

$$\Delta\mathrm{Osm} \equiv \mathrm{Osm}\,(m_2, m_3) - \mathrm{Osm}\,(m_2) - \mathrm{Osm}\,(m_3) \quad (3)$$

where m_3 and m_2 refer to the molality of urea (component 3) or KDMP (component 2) in solutions containing both solutes or just one solute. The slope of a plot of ΔOsm *vs.* the product $m_2\ m_3$ is O_{23}/RT (15, 23).

The solubilities of some bases and nucleosides as a function of urea concentration have been reported (11); we have used these data to find μ_{23}. The data were re cast in molal units using literature data for the densities of urea solutions (24). Plots of solubility *vs.* m_3 were fit to third or fourth order polynomials, as needed to obtain random residuals. The limiting slope at $m_3 = 0$ is the quantity $(\partial m_2/\partial m_3)_{\mu 2}$, where μ_2 is the chemical potential of the base or nucleoside at saturation in the absence of urea. $(\partial m_2/\partial m_3)_{\mu 2}$ and μ_{23} are related by the Euler chain rule:

$$\mu_{23} = -\mu_{22}\left(\frac{\partial m_2}{\partial m_3}\right)_{\mu_2} \quad (4)$$

μ_{22} is the self-interaction term, $(\partial\mu_2/\partial m_2)_{m3}$, which is approximated by

$$\mu_{22} \approx \frac{RT}{m_2}\left(\frac{\partial Osm}{\partial m_2}\right)_{m_3} \quad (5)$$

(see reference (9)). $(\partial\mathrm{Osm}/\partial m_2)_{\mathrm{m3}}$ should be evaluated in the absence of urea ($m_3 = 0$) at the solubility limit of m_2, but is measurable (by VPO) only at lower m_2 concentrations. The derivative must either be extrapolated to the desired m_2, or based on measurements with more soluble compounds. We have therefore estimated $(\partial\mathrm{Osm}/\partial m_2)_{\mathrm{m3}}$ for adenine or cytosine from VPO data reported for purine (an unusually soluble base) or cytidine, respectively (25). These estimates for $(\partial\mathrm{Osm}/\partial m_2)_{\mathrm{m3}}$ differ from unity (ideal behavior with no self-interaction) by at most 4.2%. $(\partial\mathrm{Osm}/\partial m_2)_{\mathrm{m3}}$ values for ribonucleosides tend to deviate more strongly from ideal behavior. VPO data reported by (35) for inosine and purine ribonucleoside gave similar values of $(\partial\mathrm{Osm}/\partial m_2)_{\mathrm{m3}} \approx 0.90$, which was used to calculate the guanosine μ_{23}. VPO data for deoxyadenosine (35) showed the largest deviations from non-ideality; extrapolation of the osmolality curve gave $(\partial\mathrm{Osm}/\partial m_2)_{\mathrm{m3}} = 0.75$. The uncertainties in $(\partial m_2/\partial m_3)_{\mu 2}$ vary from ~1% (cytosine) to ~4% (guanosine and adenine). Errors associated with $(\partial\mathrm{Osm}/\partial m_2)_{\mathrm{m3}}$ values are likely to be similar or larger because they are estimated rather than measured directly; the value for adenosine is the most problematic.

The solubility of benzene in urea solutions was analyzed in a similar way, starting from quadratic equations expressing the mole fraction solubility of benzene as a function of temperature in 0, 1, 2, 4, and 8 molar urea solutions provided by (26). Hovorka et al (27) have measured infinite dilution activity coefficients (γ_2) of benzene in urea solutions at 10, 20, 30, and 40 °C, from which we interpolated $\mu_{23} = (\partial\ln\gamma_2/\partial m_3)_{\mathrm{m2}}$ at 25 °C.

SASA calculations and unfolded RNA models

All solvent-accessible surface areas (SASA) were calculated from PDB files by the program Surface Racer (28) with the Chothia atomic radii (29) and a 1.4 Å radius probe. Files used for the RNA native structures were: A-riboswitch, 1Y26; tar-tar*, 2LJT; TLR, 2JYF (see Figure 1 for RNA names). 1TLR was used for the internal loop of the tetraloop receptor in the absence of bound tetraloop; surface areas were calculated from each of the 20 deposited coordinate files and averaged. The surface areas for helical and single strand RNA based on average A-form coordinates, and for an extended single strand averaged from non helical segments of RNA crystal structures, have been described (14). Average helical surface areas were also obtained from the following helical structures found in crystal structures: G14-A19 and U77-U82 of the A-riboswitch (1Y26); G16-U19 of the M-box riboswitch, 2QBZ; G2-G6 and A13-C17 of the A chain of a kissing loop (2JLT).

Results

RNA stability as a function of KCl and urea concentrations

Four different RNA sequences were selected for analysis (Figure 1). They were chosen to represent a range of structural complexity, from a simple hairpin to more intricate tertiary structural motifs. The selected structures are also stable in the presence of moderate concentrations of monovalent cations alone; we wished to avoid (for the present) the additional dimension of analysis that would arise if Mg^{2+} were required. We have previously determined the stability of each of the RNAs in the absence of osmolyte, by thermal denaturation. The hairpin unfolds to single stranded RNA in a single transition, and in the others, unfolding of the tertiary structure is well-resolved from the denaturation of secondary structure at higher temperatures (14, 20). For the latter three RNAs, we have only analyzed the first, tertiary structure unfolding transition; models of the partially unfolded state of each RNA are discussed below. The native structure of the adenine-riboswitch (A riboswitch, Figure 1D) is found only in its complex with adenine, which extensively stacks and hydrogen bonds with the RNA. The bound ligand, however, does not introduce any types of structure or surfaces for urea interaction that are not already commonly found in RNA tertiary structures.

An example set of melting curves for the A-riboswitch is shown in Figure 2A, and the dependence of the reciprocal RNA melting temperature on urea concentration is displayed for each of the RNAs in Figure 3A-D. (Only the first unfolding transition is plotted for each RNA.) In the ranges tested, up to 2.5 *m* urea, there was a linear relation between stability and urea concentration. The slopes of these plots are summarized in Table 1 as *m*-values, which we define here as $\mathrm{d}\left(\Delta G^{\circ}_{\mathrm{unfold}}\right)/\mathrm{d}\left(m_{\mathrm{urea}}\right)$. (The observed unfolding free energy, $\Delta G^{\circ}_{\mathrm{unfold}}$, was obtained from $1/T_m$ values by use of the average ΔH° of unfolding determined from the melting profiles.) The *m*-value for protein denaturation was originally defined in terms of a molar concentration scale (4). In this work we use molal units for the *m*-value, in part because it simplifies the separation of salt and urea effects on RNA stability.[1]

RNA structures tend to be strongly stabilized by salt. Whether the effects of urea and salt on stability are additive was tested by measuring the K^+ concentration-dependence of the stability of each RNA in the presence or absence of 2 *m* urea (Figure 4A-D). After correction for the concentration dependence of the KCl activity coefficient (21), the slope of

[1]The urea activity coefficient (γ_3) on the molar concentration scale is ~1 up to 10 M, while the corresponding molal scale activity coefficient decreases substantially with increasing urea concentration (1, 2). The decrease in $\ln(\gamma_3)$ is sufficiently close to linear that plots of RNA stability appear linear whether urea activity or urea concentration (molal scales) is used for the x-axis. The slopes of Figure 3 plots would be 16% steeper if data were plotted with respect to urea activity.

such a plot is related to the total number of ion pairs ($K^+ + Cl^-$) 'released' by the RNA upon unfolding (19, 20); this measurement is listed in Table 1 as $2\Delta\Gamma_{\pm}$ (see section on KCl – urea interactions below). For each RNA, the salt-dependence is steeper (more negative) in the presence of urea by an average of ~20%. The *m*-value itself is therefore salt dependent; the implied dependences are plotted in Figure 5 and listed in Table 1 as ∂(*m*-value)/$\partial\ln(m_{K+})$ evaluated at 2 *m* urea.

m-values determined by thermal denaturation assume that urea – RNA interactions vary negligibly over the temperature range used, and that the ΔH° used to extrapolate stability to a common temperature is itself temperature independent. To check these assumptions, we carried out isothermal titrations of the A-riboswitch RNA (initially in its native conformation bound to a purine derivative) with urea (Figure 2B). Titration conditions were adjusted to obtain well-defined low and high-concentration baselines; the final buffer included 100 m*m* KCl. The *m*-value obtained was about 18% larger than the one based on thermal measurements, which was measured with 200 m*m* KCl (Table 1). However, after taking into account the salt-dependence of the *m*-value (Figure 4C), there is excellent agreement between the two measurements (Table 3). Although isothermal titrations have the advantage that ΔH° of unfolding, which usually has a significant error, does not enter into calculation of the *m*-value, the relatively small *m*-values we measure (0.35 – 1.14 kcal/mol/*m*) generally make the titration curves too broad to analyze convincingly over the accessible urea concentration range. An advantage of melting experiments is that the effects of urea are easily detected at relatively low concentrations (< 1 *m*). Only a fairly narrow temperature range (10 – 15 °C in Figure 3) need be used to obtain the *m*-value, minimizing any temperature dependent errors.

m-values for urea interaction with model compounds

Measurement methods—Studies on the mechanism of urea-induced protein denaturation have benefited from measurements of urea interactions with amino acids and backbone model compounds, from which transfer free energies or interaction potentials have been deduced for side chains and peptide units (7, 9, 30, 31) or C, N, and O in different bonded states (8). An underlying assumption in these studies is that the overall free energy of urea - protein interactions can be parsed into additive contributions from the various chemical moieties exposed to solvent at the native or unfolded protein surfaces. Here, we use measurements from several sources to deduce similar parameters for the base, sugar, and phosphate components of RNA.

Two main experimental approaches have been used to detect interactions between two solutes in an aqueous solution, *viz.* solubility of a compound as a function of denaturant concentration (30, 32) and osmometric methods that measure water vapor pressure in equilibrium with solutions containing varying amounts of the solutes (23). Either type of experiment can quantify pairwise interactions between two solutes in terms of the same thermodynamic parameter (9). Using the notation of the Record group (8, 23, 33), the parameter is

$$\mu_{23}=RT\left(\frac{\partial\mu_2}{\partial m_3}\right)_{m_2}=RT\left(\frac{\partial\ln\gamma_2}{\partial m_3}\right)m_2 \quad (6)$$

where μ_2 and γ_2 are the chemical potential and activity coefficient of the model compound (component 2), respectively, and m_2 and m_3 are the molalities of model compound and urea (component 3), respectively. μ_{23} quantifies how strongly the chemical potential of one solute changes as a second solute is added. It is positive or negative when interactions are unfavorable or favorable, respectively; if μ_{23} is zero the two solutes interact similarly with

each other as with water. (Interactions between solutes must be reciprocal, $\mu_{23} = \mu_{32}$.) μ_{23} is a derivative of free energy with respect to two different solute concentrations, and has units cal/(mol component 2)/(*m* component 3). We will refer to it as an "interaction potential". We also report a normalized potential per unit solvent accessible surface area, μ_{23}/(SASA), for urea interactions with different types of model compounds and RNA molecular surfaces. This parameter is related by a factor of RT to the "surface interaction potential" used by Guinn *et al.* (8). Computation of SASA from molecular coordinates is described in Materials and Methods. For some purposes it becomes necessary to distinguish two contributions to μ_{23}, one from ideal mixing entropy and the other an "excess" μ_{23} due to interactions (9). In the instances considered here, this correction is small and has not been included.

Bases and nucleosides—Solubility data for bases and nucleosides as a function of co-solvent concentration have been reported for urea and other osmolytes (11, 34). We have re-calculated the data for urea in molal units and, from polynomials fit to plots of solubility *vs.* urea concentration, obtained slopes extrapolated to zero urea concentration (Figure 6A). These slopes are related to μ_{23} (eq 3). Nucleic acid bases form indefinite stacks in aqueous solutions (35), a "self-interaction" which potentially biases the effect of urea on base solubility. We have introduced a correction for this bias derived from available osmotic data for bases and nucleosides (25, 35) (see further details in Materials & Methods). μ_{23} for the various compounds are listed in Table 2. There are larger uncertainties associated with the guanosine μ_{23} measurement than with the others, for two reasons. First, the solubility curve is strongly curved (Figure 6A), which introduces more uncertainty in the slope extrapolated to zero urea. Second, guanosine has a strong propensity to form gels with stacked, hydrogen bonded structures (36), a factor not reflected in our estimates of μ_{22}.

Because urea potentially interacts with bases both by hydrogen-bonding and by stacking (37), it is important to know how strongly urea interacts with an aromatic compound that lacks hydrogen bonding capability. The solubility of benzene in aqueous urea solutions has been determined by measurement of the benzene vapor pressure (27) and by freezing point depression (26). The two studies give similar values of μ_{23} at 25 °C. The interaction potential per $Å^2$ is about half the value found for adenine and cytosine bases (Table 2), suggesting that edge-on hydrogen bonding of urea with bases is stronger than stacking between surfaces. We note as well that μ_{23} for urea interaction with the peptide unit has been measured as −0.63 cal/mol/*m*/$Å^2$ (9), similar to the interaction potential with bases.

We will argue below that bases remain relatively well-stacked in single-stranded regions of partially unfolded RNAs, and that changes in solvent accessibility at the base edges is a much larger contributor to urea-RNA interactions than urea stacking with bases. We have therefore retained a larger value of μ_{23}/SASA for bases, −0.68 cal/mol/*m*/$Å^2$, and have not attempted to differentiate base edges from base stacking surfaces in our models of partially unfolded RNAs.

Ribose—Osmometric measurements of urea with glycerol and sucrose have yielded similar values of the interaction free energy normalized for sugar SASA, μ_{23}/SASA ≈ −0.12 cal/mol/*m*/$Å^2$ (Table 2) (8, 38). The hydroxyl group is responsible for most of the interaction potential, as it both contributes the most surface area and has stronger interactions with urea than does aliphatic carbon (8). In our simple models of RNA interactions with urea, we apply this μ_{23}/SASA value derived from sugars to the total ribose SASA.

The difference between μ_{23} values of adenosine and adenine (Table 2) should be principally due to the presence of ribose in the former. After correcting for the reduced solvent accessibility of adenine when it is incorporated into adenosine, we obtain a value of −0.19 cal/mol/*m*/$Å^2$ for the interaction free energy per $Å^2$ of solvent accessible ribose. This is

more negative than the measurements with sugars (−0.12 cal/mol/*m*/Å^2) but reasonably consistent with them; the errors in adenine or adenosine μ_{23} values are amplified when subtracting out the small ribose contribution. As the sugar – urea VPO measurements are a more direct route to the μ_{23}/SASA value for CHOH surfaces, we have kept the smaller value.

KCl—Because K^+ - Cl^- pairs of ions are released upon RNA folding, any strong interaction of urea with these ions should (by LeChâtelier's principle) shift the folding equilibrium. A small, favorable μ_{23} for KCl – urea interaction has been measured (33) (Table 2). Though μ_{23} for KCl is much weaker than for adenine or cytosine bases, it is much more negative than for a 2' OH in an A form RNA duplex (~29 Å^2, −4.3 cal/mol/*m*).

Phosphate—As we knew of no prior measurements relevant to the interaction of urea with anionic phosphate oxygens, we carried out VPO studies of urea with the model compound potassium dimethylphosphate (KDMP) and found a moderately unfavorable interaction potential, μ_{23} = 41.7 ± 7.0 cal/mol/*m* (Figure 6B). The measurement does not distinguish between urea interactions with K^+ and DMP^- ions. Guinn *et al* (8) conclude from their measurements of urea interactions with various carboxylate zwitterions and carboxylate salts that μ_{23} for the K^+ cation is unfavorable, 86 cal/mol/*m*. Including small favorable interactions of urea with the methyl groups and ester oxygen (based on aliphatic carbon and hydroxyl μ_{23} values from Guinn *et al.*), we estimate μ_{23} for anionic PO_2^- as −30 cal/mol/*m*. This value of μ_{23}, when normalized per Å^2 of PO_2^- SASA (Table 2), is between the estimates for carboxylate oxygen (−0.24 cal/mol/*m*/Å^2) and carbonyl oxygen (−0.51 cal/mol/*m*/Å^2) made by Guinn *et al* (8).

Poly(A)—Hong *et al.* (39) used VPO to find that net urea interactions with helical DNA are negligible (4 ± 4 cal/mol/*m*, reported per nucleotide). Because urea denatures helical DNA, the measurement implies a net favorable interaction between urea and single-stranded DNA, presumably with the base surfaces exposed upon denaturation. However, our VPO measurements with urea and single-stranded poly(A) yielded $\mu_{23} \approx 0 \pm 39$ cal/mol/*m* (Figure 6C and Table 2), similar to the result with helical DNA. The error associated with this value is large because of the limited concentration of poly(A) with which it is feasible to work. We also measured poly(A) interactions with trimethylamine oxide (TMAO), an osmolyte strongly excluded from phosphate surfaces (15). μ_{23} is highly unfavorable, 438 cal/mol/*m* (Figure 6C). These results are rationalized in the next section.

Models of RNA unfolded states and calculation of *m*-values based on surface areas

General approach—We next ask if our parameters for urea interactions with base, ribose, and phosphate surfaces (Table 2) can be used to estimate *m*-values for unfolding of an RNA. Our approach is the same as used by others in studies of osmolyte effects on protein stability. *m*-values for macromolecular denaturation by urea are given by

$$m - \text{value} = \frac{d\left(\Delta G^{O}_{obs}\right)}{d\left(m_3\right)} = \Delta\mu_{23} \quad (7)$$

where ΔG°_{obs} is the free energy of macromolecule unfolding and $\Delta\mu_{23}$ is the difference between μ_{23} values of the unfolded and native macromolecule (component 2 in this case is the macromolecule) (23). For our calculations of *m*-values, we assume $\Delta\ \mu_{23}$ for RNA unfolding is the simple sum of contributions from changes in the exposure of different types of surfaces,

$$(\Delta\mu_{23})_{\text{RNA unfolding}} = \sum_i \left(\frac{\mu_{23}}{\text{SASA}}\right)_i \Delta(\text{SASA})_i + \Delta\Gamma_{\pm}\mu_{urea-KCl} \quad (8)$$

where the index i refers to the $\Delta\mu_{23}$/SASA ratio for phosphate, ribose, and base (Table 2). The last term accounts for any interaction of urea with pairs of K^+ - Cl^- ions released upon RNA unfolding (see Materials & Methods for the definition of $\Delta\Gamma_{\pm}$).

The solvent accessible surface area of each type of surface in the native tertiary structure can be calculated from available atomic-resolution models for three of the RNAs studied here. The more problematic task is to devise surface area models for the partially unfolded state; though attempts are being made to characterize the ensemble of states from which various RNA tertiary structures fold, the models must be considered tentative at present (40, 41). We noted that, for many RNAs, loss of tertiary structure leaves a molecular configuration consisting of helical segments joined by nominally single-stranded RNA. As a simple first approximation, we divide an unfolded RNA sequence into helix and single strand nucleotides and approximate the total SASA as the sum of average values for either conformation.

For helical segments, we either found the average surface area in an A-form helix generated by a standard set of angles, or took the average SASA of several helical segments extracted from RNA crystal structures. The two sets of numbers are essentially indistinguishable (Table 3). For single-stranded RNA, we initially devised two models with extremes in the extent of base stacking. The maximally stacked model used standard A-form RNA coordinates. To obtain a maximally extended strand, we extracted segments of unstacked nucleotides from RNA crystal structures. The extended model has increased base and ribose exposure compared to the A form model, but also shows a small decrease in phosphate exposure (Table 3). In the following section, we use these basic models of helical and single-stranded RNAs to construct simple models of unfolded RNAs for comparison with experimental data.

Poly(A)—For insight into an appropriate model for urea interaction with single-stranded RNA surfaces, μ_{23} measured for poly(A) (Table 2) was compared with the maximally stacked (A-form) and extended models of single stranded RNA described above (Table 4 and Figure 7). To account for urea interactions with mobile ions, we use the excess ion values inferred from experiment by Bond *et al.* (42) for single stranded phage DNA: at the equilibrated K^+ concentration used in the VPO experiments, $\Gamma_+ \approx 0.8$ and $\Gamma_- \approx -0.2$. In both models large favorable interactions of urea with base and phosphate are partially cancelled by the net unfavorable interactions with mobile ions. The model based on A-form RNA gives a value of μ_{23} nearly identical to the experimental measurement, though because of the large errors the extended model cannot be ruled out. Careful studies of poly(A) hyperchromicity suggest that adenine stacking is at about 90% of maximum at 25 °C (43), consistent with the A-form model better describing urea interactions.

Hairpin—Unfolding of the hairpin converts 12 helical nucleosides to a single-stranded conformation (5′ and 3′ terminal bases are stacked on one side only in both conformations). The U_4 hairpin loop sequence was chosen to be minimally stacked; for a first approximation we consider it unchanged in average conformation after unfolding. If the stacked, A-form model is used for single strands, the backbone remains unchanged upon denaturation and only base surface area becomes more exposed. The more extended model for single-stranded RNA leads to contrasting behavior, in which denaturation increases both base and ribose accessible surface areas and phosphate surfaces becomes slightly less accessible. Applying our μ_{23}/SASA parameters, the A-form model is within error of the experimental *m*-value

(Table 4 and Figure 7) while the extended model gives a much more negative *m*-value. Taken at face value, the calculation implies that single-stranded RNA is much closer to A-form geometry than to an extensively unstacked strand, a reasonable conclusion given the propensity of bases to remain stacked (44) and the agreement of an A-form single-strand model with the poly(A) VPO measurements. Based on these results, we use the A-form single strand model in all the subsequent RNA tertiary structure models. tar tar*. The structure of a kissing loop complex, differing from the sequence in Figure 1 by only stem base pairs, has been reported (2JLT, (45)). In the complex, the loop backbone makes a tight bend that brings two phosphates into proximity (oxygens as close as 4.5 Å), and hydrogen bonds form between a phosphate on one strand and a 2′ hydroxyl on the other. Thus, two phosphates on each strand have reduced accessibility to water compared to phosphates in A-form helices (SASA ~40 $Å^2$ vs. 69 $Å^2$, per PO_2^-, respectively), potentially providing a test for the anionic oxygen free energy parameter.

For the unfolded state, we model each hairpin in two ways. In one, we assume that the 6 nt hairpin loop of each RNA adopts (on average) the A-form single-strand RNA conformation. This model purposely ignores the fact that at least one base stack must be completely disrupted to make a 180° turn in the backbone; it therefore should underestimate base exposure and the *m*-value. The second model adds in the additional base and sugar exposure of a 5′ and 3′ terminal nucleotide as a way to approximate nucleotide exposure at the turn in the hairpin loop. The *m*-value of the latter model is within error of the experimental value, while the first model has a less negative value than measured, as expected. According to the models, more than 80% of the observed *m*-value is derived from changes in bases exposure and only ~9% from phosphate interactions. Changes in the accessibility of RNA phosphates to urea are not negligible in computing *m*-values, though denaturation is clearly dominated by urea interactions with bases.

A-riboswitch—The A-riboswitch aptamer is structurally the most complex of the RNAs studied here. Studies utilizing various spectroscopic (x-ray scattering, fluorescence energy transfer, and NMR) and chemical probes have shown that, in the absence of Mg^{2+}, major conformational changes take place upon removal of the adenine ligand: the two hairpin loops become completely separated, the three helix junction adopts an extended structure that probably maintains extensive stacking, and the binding pocket undergoes substantial rearrangement to a less compact structure (46-50). We use similar models as for the tar-tar* complex to model the unfolded state of this RNA: one model assumes fully stacked A-form single strands throughout non-helical regions, the other allows for nucleoside exposure at turns in the two hairpin loops. The division of the RNA into helical and single strand segments is shown by the boxes in Figure 1D. The model with less stacking is well within experimental error of the measured *m*-value (Table 4 and Figure 7).

TLR RNA—The TLR RNA (Figure 1) was designed (51) to dimerize *via* the common tetraloop - receptor tertiary structural motif. A high resolution NMR-based model of the dimer (52) shows the tetraloop - receptor contacts expected from crystal structures of RNAs containing the motif (53): inter-strand contacts between the tetraloop hairpin (G20 – A24, Figure 1C) and the receptor (bracketed internal loop) are almost entirely base – base hydrogen-bonding and stacking. A reason for selecting this RNA for study is that structural information about the receptor sequence in the absence of a bound tetraloop is available (54), providing an experimental model of the unfolded state to compare with our simple helix/single strand models.

The GAAA tetraloop itself is a stable structure that does not undergo any significant change in conformation upon docking into the receptor (55). NMR studies found that the free receptor motif adopts an alternate stacking pattern (54) in which the total SASA of the bases

is not significantly different from base exposure calculated for the native receptor in the absence of the tetraloop. Using a model for monomeric TLR RNA based on the NMR data, we find more than half of the total SASA changes coming from riboses that become buried at the tetraloop - receptor interface; this fraction is much higher than for any of the other RNAs studied here (Table 4). This RNA also has the largest number of released ion pairs of the RNAs studied here, probably because the parallel helices in the dimer create a region of high charge density (20). This structure-based model gives a calculated *m*-value that underestimates the experimental value by about 20% (Figure 7).

We also used the simple average A-form helix and single strand parameters to make two models of the receptor that should bracket the actual surface area exposure. The receptor is an asymmetric internal loop, AU for one strand and UAA for the other. The model with minimal surface area exposure uses helical SASA parameters for all the internal loop nucleotides; the corresponding model with maximum SASA exposure uses the A-form single strand parameters. *m*-values for both the NMR-based model and the measurement fall in between the *m*-values derived from the two models (Figure 7). Thus, we would have been able to provide reasonable limits for the *m*-value in the absence of structural information.

Discussion

General comments

In this work we have quantified the effects of urea on RNA secondary and tertiary structure, and devised a simple model that accounts for the RNA destabilization in terms of urea interactions with RNA surfaces. We took a similar approach as successfully used in studies of urea induced protein denaturation (5-8), and devised a set of interaction potentials for urea interactions with base, ribose, and phosphate surfaces from experiments with small molecule mimics of RNA components. These parameters, when combined with models of solvent accessible RNA surfaces, account remarkably well for urea induced destabilization (*m*-value) of RNA secondary structure and several RNA tertiary structures, as well as for urea interaction with poly(A). The success of the approach used to estimate the exposed surface areas of unfolded RNAs was unexpected, given the simplicity of the models and the potential difficulty of the problem. The correspondence we find between measured and calculated interactions of urea with RNA has several implications:

First, our calculations assume that urea interaction potentials with base, ribose, and phosphate components of an RNA are additive and proportional to the respective accessible surface areas. Similar assumptions work well for urea-induced protein denaturation (5, 7, 9), but the intense electrostatic potential at an RNA surface, the surrounding excess of cations, and networks of hydration between phosphates are all factors, not found in proteins, that alter solution properties near an RNA surface and might have made an additive, surface area approach too simplistic.

Second, a model of the RNA unfolded state as a combination of well-stacked single strand and helical conformations works surprisingly well, which implies that RNA bases have a strong tendency to remain stacked in the unfolded state. It was evident from the first RNA crystal structures that RNAs adopt maximally stacked structures even in single-stranded hairpin loops or terminal single strand extensions (56, 57). Bulges, asymmetric internal loops, and complex junction loops may prove less amenable to our simple modeling, but it is likely that it will be possible to place maximum and minimum limits on the surface area exposures, a strategy successfully used to model protein unfolded states (58, 59).

Third, urea interaction with RNA bases is the single largest term responsible for urea-induced denaturation of RNA: urea – base interactions are the strongest in terms of free

energy per square Ångstrom of surface area, and bases comprise 50 – 100% of the total surface area change upon RNA unfolding. However, urea interactions with backbone and released ions are not negligible; they constitute about a third of the destabilizing free energy for the TLR RNA.

Comparison of *m*-values with previous studies of RNA and proteins

In a study of the stabilities of RNA duplexes and tRNA in urea, an average *m*-value/ΔSASA of −0.099 cal/mol/M/Å^2 was found (12). The *m*-value/ΔSASA for our four RNAs are much larger, −0.48 (A riboswitch) to −0.65 (hairpin) cal/mol/*m*/Å^2 (from Table 4 data using ΔSASA from the model that gives a calculated value closest to the measured value). The difference in urea concentration units (M vs. *m*) does not account for the 5-6 fold difference. Much of the discrepancy can be attributed to the assumption in (12) that single-stranded RNA in urea adopts the maximum surface area exposure allowed by stereochemistry (60); the accessible surface areas are even larger than those of our 'extended' model. Our results, particularly with poly(A), are inconsistent with such extreme unfolding of the RNA.

Urea interacts favorably with all protein surfaces, both backbone and side chains (7). The strongest interaction per Å^2 of accessible surface area is with backbone amide, found to be −0.63 cal/mol/*m*/Å^2 (9); backbone interactions are also the largest single contributor to the *m*-value (7). Thus, the strength of the urea – backbone interactions in proteins are comparable to urea – base interactions in RNA. The average *m*-value/ΔSASA ratio for protein unfolding has been reported as −0.11 or −0.14 cal/mol/M/Å^2 (5, 61), which is smaller in magnitude than we find for RNA. The difference arises because the majority of the surfaces exposed by RNA denaturation are the strongly-interacting bases, while a large fraction of surfaces exposed by protein denaturation are weakly interacting side chains.

RNA unfolded states and the salt-dependence of the *m*-value

The observation that *m*-values decrease with salt concentration (Figure 5) is equivalent to stating that urea increases the extent of ion release upon RNA unfolding (cf. the steeper salt-dependences of unfolding obtained in the presence of urea, Figure 4). We think this thermodynamic coupling between salt and urea can be traced to their interactions with the unfolded state of the RNA. Because of its favorable interactions with all RNA surfaces, urea is expected to favor more extended conformations of unfolded RNA. Extended conformations have lower charge densities and thus lower accumulation of excess ions. (The weakly favorable interaction between urea and KCl should also favor release of salt, and thus unfolding to RNA conformations with lower charge densities.) A rough estimate of the magnitude of this effect for denaturation of an RNA helix to single-stranded RNA can be made from Manning's counterion condensation theory (62), which relates Γ_+, the fraction of polynucleotide charges neutralized by excess cations, to the linear spacing of charges in a polynucleotide (19). Γ_+ for an A-form helix, with two charges every 2.9 Å, is 0.95 cations/nucleotide; for a single strand with 3.4 Å spacing between charges (42), Γ_+ is 0.88. The difference between these two numbers is the cation release upon unfolding, $\Delta\Gamma_+ = -0.07$ cations per nucleotide. (The change in anion exclusion per nucleotide, $\Delta\Gamma_-$, is necessarily the same number.) A 20% increase in $\Delta\Gamma_+$ requires only a modest ~10% increase in the phosphate spacing of the single-stranded form. Counterion condensation theory was derived for long, linear polymers and does not directly apply to short oligomers or the irregular RNA structures considered here, but the above calculation suggests that only modest effects of urea on the extension of unfolded RNAs could change the charge density sufficiently to account for the observed increase in salt dependence. If this argument is correct, then more realistic models of unfolded RNAs, which incorporate the influence of salt and urea on RNA dimensions and charge density, would allow *m*-value calculations to be made for a specific set of ionic conditions.

At present, the lack of detailed descriptions of the ensemble of unfolded conformations from which an RNA folds is a limiting factor in parsing the energetics of RNA folding. Experimental and computational approaches are being brought to bear on the problem (40, 41). In this regard, we note the potential of the osmolytes TMAO and urea to provide additional information about the types of surfaces exposed to solvent by RNA denaturation. The two osmolytes function by fundamentally different mechanisms: TMAO stabilizes RNA principally by unfavorable interactions with the RNA backbone, and also decreases the dependence of the unfolding free energy on salt concentration by promoting compact conformations of unfolded RNAs (15). TMAO and urea thus probe RNA surfaces in largely complementary ways, with the potential to provide a quantitative perspective on the conformational changes taking place in RNAs upon denaturation.

Acknowledgments

We thank Robert Trachman for useful comments and discussion.

This work was supported by National Institutes of Health Grant 1RO1 GM58545.

Abbreviations used

VPO	vapor pressure osmometry
Osm	osmolality
KDMP	potassium dimethylphosphate
SASA	solvent accessible surface area
TMAO	trimethylamine oxide

References

1. Scatchard G, Hamer WJ, Wood SE. Isotonic Solutions. I. The Chemical Potential of Water in Aqueous Solutions of Sodium Chloride, Potassium Chloride, Sulfuric Acid, Sucrose, Urea and Glycerol at 25°. J Am Chem Soc. 1938; 60:3061–3070.
2. Rosgen J, Pettitt BM, Bolen DW. Uncovering the basis for nonideal behavior of biological molecules. Biochemistry. 2004; 43:14472–14484. [PubMed: 15533052]
3. Tanford C. Isothermal Unfolding of Globular Proteins in Aqueous Urea Solutions. J Am Chem Soc. 1964; 86:2050–2059.
4. Greene RF Jr. Pace CN. Urea and guanidine hydrochloride denaturation of ribonuclease, lysozyme, alpha-chymotrypsin, and beta lactoglobulin. J Biol Chem. 1974; 249:5388–5393. [PubMed: 4416801]
5. Myers JK, Pace CN, Scholtz JM. Denaturant m-values and heat capacity changes: relation to changes in accessible surface areas of protein unfolding. Protein Sci. 1995; 4:2138–2148. [PubMed: 8535251]
6. Courtenay ES, Capp MW, Saecker RM, Record MT Jr. Thermodynamic analysis of interactions between denaturants and protein surface exposed on unfolding: interpretation of urea and guanidinium chloride m values and their correlation with changes in accessible surface area (ASA) using preferential interaction coefficients and the local bulk domain model. Proteins Suppl. 2000; 4:72–85.
7. Auton M, Bolen DW. Predicting the energetics of osmolyte-induced protein folding/unfolding. Proc Natl Acad Sci U S A. 2005; 102:15065–15068. [PubMed: 16214887]
8. Guinn EJ, Pegram LM, Capp MW, Pollock MN, Record MT Jr. Quantifying why urea is a protein denaturant, whereas glycine betaine is a protein stabilizer. Proc Natl Acad Sci U S A. 2011; 108:16932–169327. [PubMed: 21930943]

9. Cannon JG, Anderson CF, Record MT Jr. Urea-amide preferential interactions in water: quantitative comparison of model compound data with biopolymer results using water accessible surface areas. J Phys Chem B. 2007; 111:9675–9685. [PubMed: 17658791]
10. Bolen DW, Rose GD. Structure and energetics of the hydrogen-bonded backbone in protein folding. Annu Rev Biochem. 2008; 77:339–362. [PubMed: 18518824]
11. Herskovits TT, Bowen JJ. Solution studies of the nucleic acid bases and related model compounds. Solubility in aqueous urea and amide solutions. Biochemistry. 1974; 13:5474–5483. [PubMed: 4549016]
12. Shelton VM, Sosnick TR, Pan T. Applicability of urea in the thermodynamic analysis of secondary and tertiary RNA folding. Biochemistry. 1999; 38:16831–16839. [PubMed: 10606516]
13. Schwinefus JJ, Kuprian MJ, Lamppa JW, Merker WE, Dorn KN, Muth GW. Human telomerase RNA pseudoknot and hairpin thermal stability with glycine betaine and urea: preferential interactions with RNA secondary and tertiary structures. Biochemistry. 2007; 46:9068–9079. [PubMed: 17630773]
14. Lambert D, Draper DE. Effects of Osmolytes on RNA Secondary and Tertiary Structure Stabilities and RNA-Mg^{2+} Interactions. J Mol Biol. 2007; 370:993–1005. [PubMed: 17555763]
15. Lambert D, Leipply D, Draper DE. The Osmolyte TMAO Stabilizes Native RNA Tertiary Structures in the Absence of Mg(2+): Evidence for a Large Barrier to Folding from Phosphate Dehydration. J Mol Biol. 2010; 404:138–157. [PubMed: 20875423]
16. Leipply D, Draper DE. The dependence of RNA tertiary structure stability on Mg^{2+} concentration: interpretation of the Hill equation and coefficient. Biochemistry. 2010; 49:1843–1853. [PubMed: 20112919]
17. Petersheim M, Turner DH. Base stacking and Base-Pairing Contributions to Helix Stability: Thermodynamics of Double Helix Formation with CCGG, CCGGp,CCGGAp, CCGGUp, and ACCGGUp. Biochemistry. 1983; 22:256–263. [PubMed: 6824629]
18. Draper, DE.; Bukhman, YV.; Gluick, TC. Current Protocols in Nucleic Acid Chemistry. Beaucage, SL.; Bergstrom, DE.; Glick, GD.; Jones, RA., editors. 2000.
19. Record MT Jr. Zhang W, Anderson CF. Analysis of effects of salts and uncharged solutes on protein and nucleic acid equilibria and processes: a practical guide to recognizing and interpreting polyelectrolyte effects, Hofmeister effects, and osmotic effects of salts. Adv Protein Chem. 1998; 51:281–353. [PubMed: 9615173]
20. Lambert D, Leipply D, Shiman R, Draper DE. The influence of monovalent cation size on the stability of RNA tertiary structures. J Mol Biol. 2009; 390:791–804. [PubMed: 19427322]
21. Leipply D, Lambert D, Draper DE. Ion–RNA Interactions: Thermodynamic Analysis of the Effects of Mono- and Divalent Ions on RNA Conformational Equilibria. Methods in Enzymology. 2009; 469:433–463. [PubMed: 20946802]
22. Archer DG. Thermodynamic Properties of the KCl+H2O System. J Phys Chem Ref Data. 1999; 28:1–17.
23. Capp MW, Pegram LM, Saecker RM, Kratz M, Riccardi D, Wendorff T, Cannon JG, Record MT Jr. Interactions of the osmolyte glycine betaine with molecular surfaces in water: thermodynamics, structural interpretation, and prediction of m values. Biochemistry. 2009; 48:10372–10379. [PubMed: 19757837]
24. Gucker FT, Gage FW, Moser CE. The Densities of Aqueous Solutions of Urea at 25 and 30° and the Apparent Molal Volume of Urea. J Am Chem Soc. 1938; 60:2582–2588.
25. Ts'o POP, Melvin IS, Olson AC. Interaction and Association of Bases and Nucleosides in Aqueous Solutions. J Am Chem Soc. 1963; 85:1289–1296.
26. Ueda M, Katayama A, Kuroki N, Urahata T. Effect of urea on the solubility of benzene and toluene in water. Progr Colloid & Polymer Sci. 1978; 63:116–119.
27. Hovorka S, Dohnal V, Carrillo-Nava E, Costas M. Infinite dilution activity coefficients for benzene and toluene in water and in aqueous solutions of the protein denaturants urea and guanidine hydrochloride. J Chem Thermodynamics. 2000; 32:1683–1705.
28. Tsodikov OV, Record MT Jr. Sergeev YV. Novel computer program for fast exact calculation of accessible and molecular surface areas and average surface curvature. J Comput Chem. 2002; 23:600–609. [PubMed: 11939594]

29. Chothia C. The nature of the accessible and buried surfaces in proteins. J Mol Biol. 1976; 105:1–12. [PubMed: 994183]
30. Nozaki Y, Tanford C. The Solubility of Amino Acids and Related Compounds in Aqueous Urea Solutions. J Biol Chem. 1963; 238:4074–4081. [PubMed: 14086747]
31. Auton M, Bolen DW. Additive transfer free energies of the peptide backbone unit that are independent of the model compound and the choice of concentration scale. Biochemistry. 2004; 43:1329–1342. [PubMed: 14756570]
32. Liu Y, Bolen DW. The peptide backbone plays a dominant role in protein stabilization by naturally occurring osmolytes. Biochemistry. 1995; 34:12884–12891. [PubMed: 7548045]
33. Hong J, Capp MW, Anderson CF, Record MT. Preferential interactions in aqueous solutions of urea and KCl. Biophys Chem. 2003; 105:517–532. [PubMed: 14499915]
34. Herskovits TT, Harrington JP. Solution studies of the nucleic acid bases and related model compounds. Solubility in aqueous alcohol and glycol solutions. Biochemistry. 1972; 11:4800–1481. [PubMed: 4540188]
35. Solie TN, Schellman JA. The interaction of nucleosides in aqueous solution. J Mol Biol. 1968; 33:61–77. [PubMed: 5646654]
36. Guschlbauer W, Chantot JF, Thiele D. Four-stranded nucleic acid structures 25 years later: from guanosine gels to telomer DNA. J Biomol Struct Dyn. 1990; 8:491–511. [PubMed: 2100515]
37. Priyakumar UD, Hyeon C, Thirumalai D, Mackerell AD Jr. Urea destabilizes RNA by forming stacking interactions and multiple hydrogen bonds with nucleic acid bases. J Am Chem Soc. 2009; 131:17759–17761. [PubMed: 19919063]
38. Ellerton HD, Dunlop PJ. Activity Coefficients for the Systems Water-Urea and Water-Urea-Sucrose at 25° from Isopiestic Measurements. J Phys Chem. 1966; 70:1831–1837.
39. Hong J, Capp MW, Anderson CF, Saecker RM, Felitsky DJ, Anderson MW, Record MT Jr. Preferential interactions of glycine betaine and of urea with DNA: implications for DNA hydration and for effects of these solutes on DNA stability. Biochemistry. 2004; 43:14744–14758. [PubMed: 15544345]
40. Grilley D, Misra V, Caliskan G, Draper DE. Importance of Partially Unfolded Conformations for Mg(2+)-Induced Folding of RNA Tertiary Structure: Structural Models and Free Energies of Mg(2+) Interactions. Biochemistry. 2007; 46:10266–10278. [PubMed: 17705557]
41. Stoddard CD, Montange RK, Hennelly SP, Rambo RP, Sanbonmatsu KY, Batey RT. Free state conformational sampling of the SAM I riboswitch aptamer domain. Structure. 2010; 18:787–797. [PubMed: 20637415]
42. Bond JP, Anderson CF, Record MT Jr. Conformational transitions of duplex and triplex nucleic acid helices: thermodynamic analysis of effects of salt concentration on stability using preferential interaction coefficients. Biophys J. 1994; 67:825–836. [PubMed: 7948695]
43. Leng M, Felsenfeld G. A study of polyadenylic acid at neutral pH. J Mol Biol. 1966; 15:455–466. [PubMed: 5915177]
44. Holbrook JA, Capp MW, Saecker RM, Record MT Jr. Enthalpy and heat capacity changes for formation of an oligomeric DNA duplex: interpretation in terms of coupled processes of formation and association of single stranded helices. Biochemistry. 1999; 38:8409–8422. [PubMed: 10387087]
45. Lebars I, Legrand P, Aime A, Pinaud N, Fribourg S, Di Primo C. Exploring TAR-RNA aptamer loop loop interaction by X-ray crystallography, UV spectroscopy and surface plasmon resonance. Nucleic Acids Res. 2008; 36:7146–156. [PubMed: 18996893]
46. Lemay JF, Penedo JC, Tremblay R, Lilley DM, Lafontaine DA. Folding of the adenine riboswitch. Chem Biol. 2006; 13:857–868. [PubMed: 16931335]
47. Noeske J, Schwalbe H, Wohnert J. Metal ion binding and metal ion induced folding of the adenine-sensing riboswitch aptamer domain. Nucleic Acids Res. 2007; 35:5262–5273. [PubMed: 17686787]
48. Gilbert SD, Love CE, Edwards AL, Batey RT. Mutational analysis of the purine riboswitch aptamer domain. Biochemistry. 2007; 46:13297–13309. [PubMed: 17960911]

49. Brenner MD, Scanlan MS, Nahas MK, Ha T, Silverman SK. Multivector fluorescence analysis of the xpt guanine riboswitch aptamer domain and the conformational role of guanine. Biochemistry. 2010; 49:1596–1605. [PubMed: 20108980]
50. Leipply D, Draper DE. Effects of Mg(2+) on the free energy landscape for folding a purine riboswitch RNA. Biochemistry. 2011; 50:2790–2799. [PubMed: 21361309]
51. Jaeger L, Westhof E, Leontis NB. TectoRNA: modular assembly units for the construction of RNA nano objects. Nucleic Acids Res. 2001; 29:455–463. [PubMed: 11139616]
52. Zuo X, Wang J, Foster TR, Schwieters CD, Tiede DM, Butcher SE, Wang YX. Global molecular structure and interfaces: refining an RNA:RNA complex structure using solution X-ray scattering data. J Am Chem Soc. 2008; 130:3292–3293. [PubMed: 18302388]
53. Adams PL, Stahley MR, Kosek AB, Wang J, Strobel SA. Crystal structure of a self-splicing group I intron with both exons. Nature. 2004; 430:45–50. [PubMed: 15175762]
54. Butcher SE, Dieckmann T, Feigon J. Solution structure of a GAAA tetraloop receptor RNA. Embo J. 1997; 16:7490–7499. [PubMed: 9405377]
55. Cate JH, Gooding AR, Podell E, Zhou K, Golden BL, Kundrot CE, Cech TR, Doudna JA. Crystal structure of a group I ribozyme domain: principles of RNA packing. Science. 1996; 273:1678–1685. [PubMed: 8781224]
56. Kim SH, Suddath FL, Quigley GJ, McPherson A, Sussman JL, Wang AH, Seeman NC, Rich A. Three-dimensional tertiary structure of yeast phenylalanine transfer RNA. Science. 1974; 185:435–440. [PubMed: 4601792]
57. Roberts RW, Crothers DM. Stability and Properties of Double and Triple Helices: Dramatic Effects of RNA or DNA Backbone Composition. Science. 1992; 258:1463. [PubMed: 1279808]
58. Creamer TP, Srinivasan R, Rose GD. Modeling unfolded states of peptides and proteins. Biochemistry. 1995; 34:16245–16250. [PubMed: 8845348]
59. Creamer TP, Srinivasan R, Rose GD. Modeling unfolded states of proteins and peptides. II. Backbone solvent accessibility. Biochemistry. 1997; 36:2832–5. [PubMed: 9062111]
60. Alden CJ, Kim SH. Solvent accessible Surfaces of Nucleic Acids. J. Mol. Biol. 1979; 132:411–434. [PubMed: 533898]
61. Hong J, Capp MW, Saecker RM, Record MT Jr. Use of urea and glycine betaine to quantify coupled folding and probe the burial of DNA phosphates in lac repressor lac operator binding. Biochemistry. 2005; 44:16896–16911. [PubMed: 16363803]
62. Manning GS. Limiting Laws and Counterion Condensation in Polyelectrolyte Solutions I. Colligative Properties. J Phys Chem. 1969; 51:924–933.
63. Chang KY, Tinoco I. The Structure of an RNA “Kissing” Hairpin Complex of the HIV TAR Hairpin Loop and its Complement. J Mol Biol. 1997; 269:52–66. [PubMed: 9193000]
64. Serganov A, Yuan YR, Pikovskaya O, Polonskaia A, Malinina L, Phan AT, Hobartner C, Micura R, Breaker RR, Patel DJ. Structural basis for discriminative regulation of gene expression by adenine- and guanine-sensing mRNAs. Chem Biol. 2004; 11:1729–1741. [PubMed: 15610857]

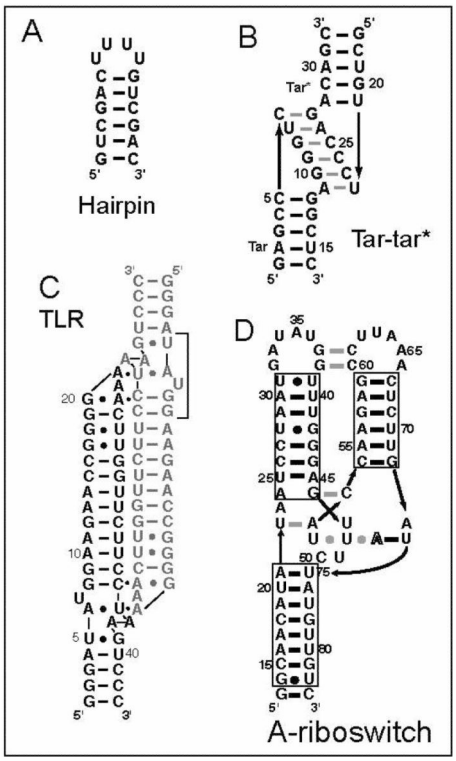

Figure 1.

RNAs used in this study. Base pairs in secondary structures are indicated by black bars or dots; tertiary hydrogen bonding between bases is denoted by gray bars or dots. **A**, designed hairpin. **B**, Tar tar* kissing loop complex (63). **C**, RNA designed to dimerize via the tetraloop - receptor (TLR) structural motif (51). The bracket indicates the receptor internal loop sequence that was substituted with PDB file 1TLR in devising the unfolded state model. **D**, aptamer domain of the adenine riboswitch (A riboswitch) (64). The base in outline is the ligand adenine. Boxes indicate presumed helical regions in the unfolded state models.

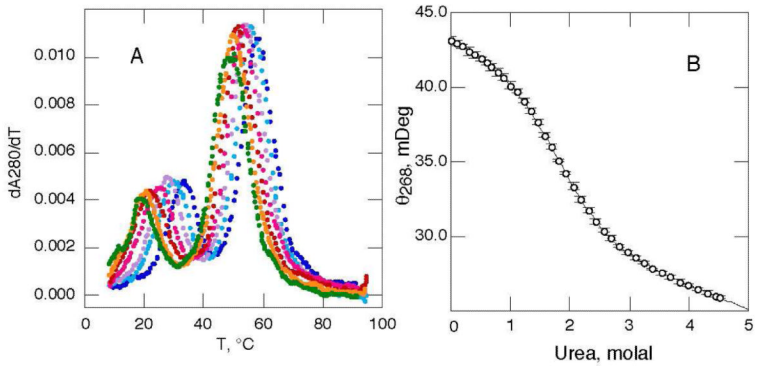

Figure 2.

Urea induced denaturation of A-riboswitch RNA. **A**, melting profiles of the RNA at various concentrations of urea, from 0 (blue) to 2.4 *m* (green) in 0.4 *m* increments. KMOPS – EDTA buffer (see Materials and Methods) also contained 200 m*m* KCl and 5 μ*m* DAP. **B**, isothermal titration (15 °C) of A-riboswitch RNA with urea. KMOPS – EDTA buffer (see Materials and Methods) also contained 100 m*m* KCl and 100 μ*m* DAP.. The curve is a least squares best fit to an equation with linear upper and lower baselines and a cooperative, two-state transition (Hill equation).

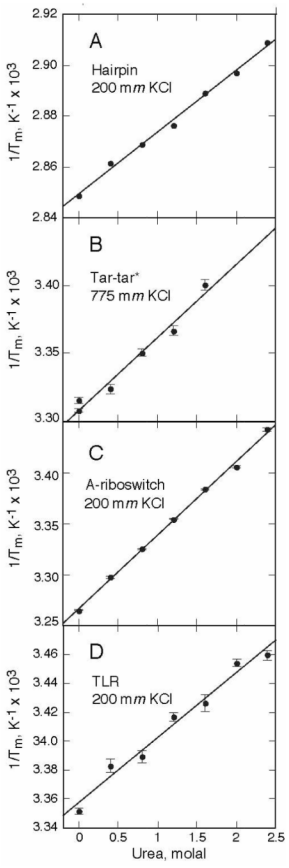

Figure 3.

Urea dependence of stabilities (T_m^{-1}) of the RNAs shown in Figure 1. T_ms are derived from melting curves such as those shown in Figure 2A, using KMOPS buffer with the KCl concentration as shown. Error bars are standard deviations based on three independent measurements; where bars are not visible, the errors are comparable to the size of the points.

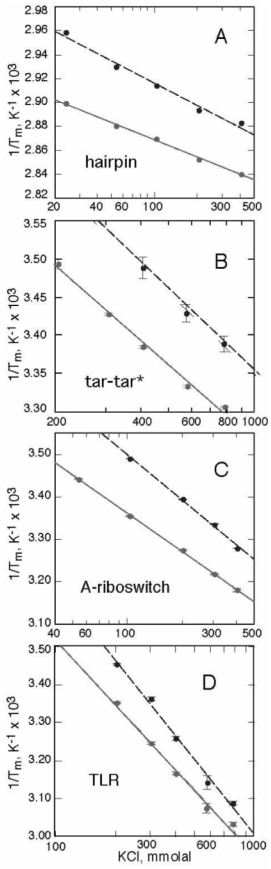

Figure 4.

Salt dependence of RNA stabilities in the presence (dashed line) or absence (continuous line) of 2 *m* urea, as derived from melting profiles carried out in KMOPS buffer with various molalities of KCl. Error bars are standard deviations based on three independent measurements; where bars are not visible, the errors are comparable to the size of the points.

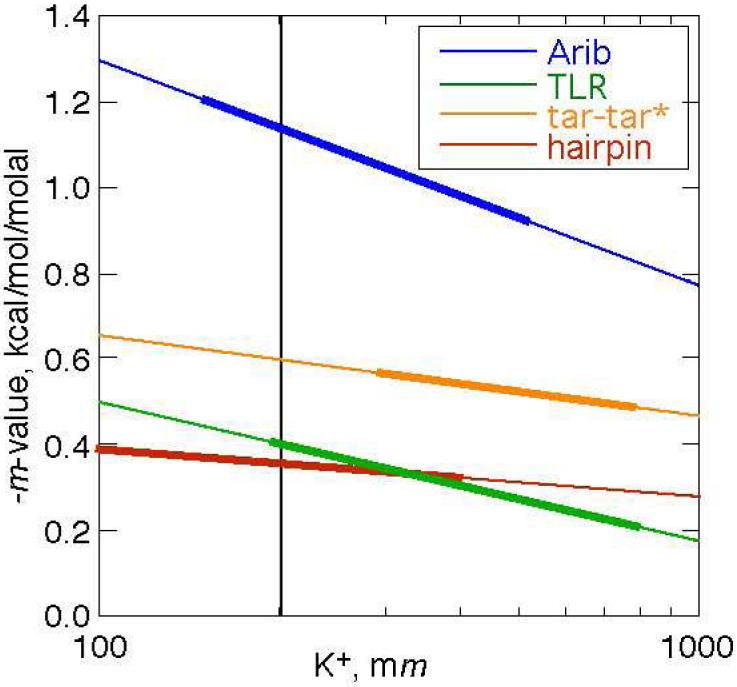

Figure 5.

Salt dependence of *m*-values. The *m*-values for each RNA were calculated from slopes of the data in Figures 3 and 4. The heavy lines indicate the salt concentration range over which data were collected; thin lines are linear extrapolations of the data. Vertical line at 204 m*m* K^+ is the total K^+ concentration at which the experimental *m*-values are compared with calculated values (Table 4). The RNAs are: blue, A riboswitch; green, TLR; orange, tar tar*; red, hairpin.

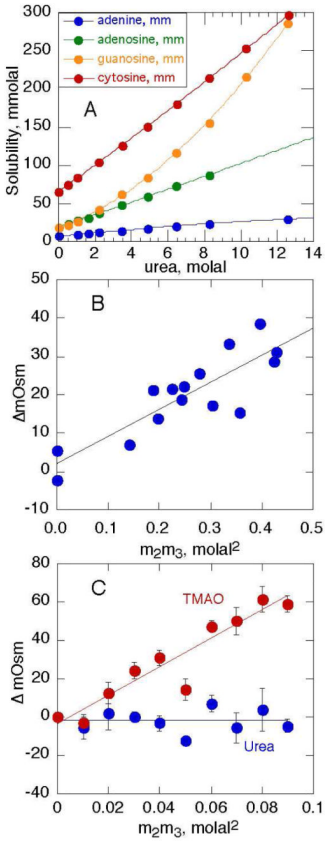

Figure 6.

Urea interactions with solutes. μ_{23} values derived from the slopes of these graphs are compiled in Table 2. **A**, solubility data from (11). Lines are fits of third order (guanosine) or second order (other compounds) polynomials, which were used to find limiting slopes at 0 *m* urea. **B**, VPO measurements for urea with KDMP. **C**, VPO measurements with poly(A) and either 1 *m* TMAO (red) or 1 *m* urea (blue). Error bars are based on three independent replicates of each point.

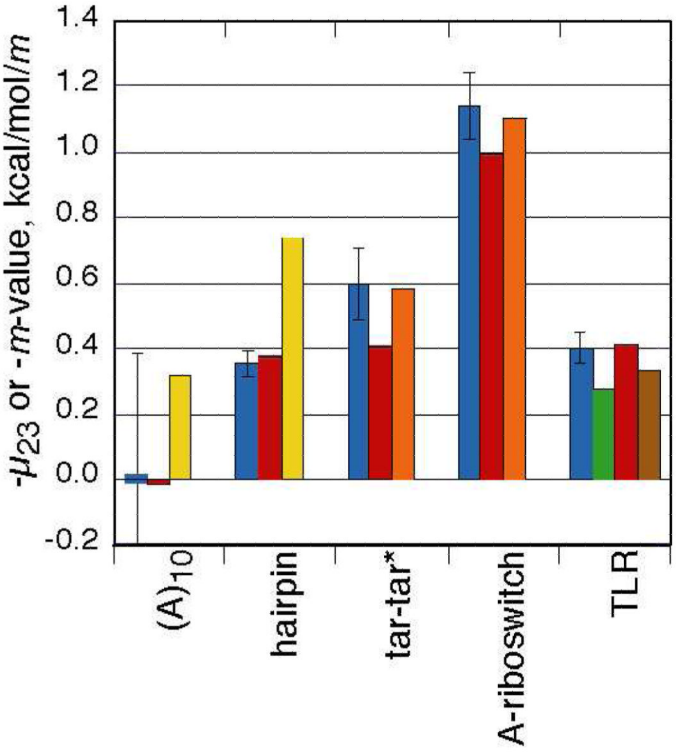

Figure 7.

Comparisons of measured RNA μ_{23} or *m*-values with those calculated from different models of the unfolded state (Tables 3 and 4). RNAs are named as in Figure 1. $(A)_{10}$ shows the μ_{23} values for poly(A) (Table 2), but reported for 10 nts. Blue bars, experimental μ_{23} or *m*-value (with errors) from Table 1. Yellow bars, μ_{23} or *m*-value calculated using the extended model for single strands. Red bars, μ_{23} or *m*-values calculated with single-stranded RNA of the unfolded state (including hairpins and internal loops) in A-form geometry. Orange bars, unfolded state models incorporate unstacked bases in hairpin loops. Green bar (TLR), internal loop of the unfolded RNA modeled as A-form helix. Brown bar (TLR), unfolded state of the receptor is a structure derived from NMR constraints (1TLR).

Table 1

RNA unfolding parameters as functions of salt and urea molality

RNA (mm KCl)	ΔH° kcal/mol[a]	*m*-value kcal/mol/molal	$2\Delta\Gamma_{\pm}$ ions/RNA	$\Delta\Gamma_{\pm}$ (2 *m* Urea) ions/RNA
hairpin (200)	49.1 ± 4.8	−0.355 ± 0.037	−0.462 ± 0.062	−0.594 ±0.092
tar-tar* (200)	29.2 ± 4.5	−0.486 ± 0.091	−1.86 ± 0.31	−2.04 ± 0.36
A-riboswitch (200)	52.9 ± 4.7	−1.14 ± 0.10	−3.07 ± 0.28	−4.07 ± 0.41
(100)[b]		−1.30		
isothermal (100)[c]		−1.34 ± 0.03		
TLR (775)	30.0 ±3.0	−0.401 ± 0.049	−3.30 ± 0.38	−3.86 ± 0.44
(200)[b]		−0.597 ± 0.11		

[a] ΔH° for RNA unfolding was averaged from all the melting profiles used in the analysis, with the exception of the TLR ΔH°, which is taken from scanning calorimetry experiments (20).

[b] *m*-value extrapolated to indicated m*m* K^+ by linear extrapolation of salt-dependences, as shown in Figure 4.

[c] *m*-value measured by isothermal titration of A-riboswitch RNA with urea (Figure 2B).

Table 2

μ23 and SASA *m*-values for model compounds at 25° C

Molecule	μ_{23} cal/mol/*m*	SASA Å^2	μ_{23}/SASA cal/mol/*m*/Å^2
adenine[a]	−176.1	265.5	−0.66
cytosine[a]	−152.1	247.7	−0.61
adenosine[a]	−173.4	423.3	−0.41
guanosine[a]	−160.4	444.6	−0.36
benzene[b]	−62.7	213.4	−0.29
benzene[c]	−65.1	213.4	−0.31
(ribose)[d]	(−38.7)	(226.4)	−0.19
glycerol[e]	−30.2	246.9	−0.122
sucrose[f]	−60.9	508.9	−0.120
KDMP[g]	−41.7 ± 7.0	85.0 (PO_2^-)	−0.36
KCl[h]	−28	-	
poly(A), per nt[i]	−0.4 ± 39		
values used for calculation of *m*-values from ΔSASA			
base			−0.64
sugar			−0.12
phosphate (PO_2^-)			−0.36

[a]Data from (11).

[b]Data from (26).

[c]Data from (27).

[d]Calculated from the difference between adenine and adenosine μ_{23} values.

[e]Data from (8).

[f]Data from (38); the same result within error (μ_{23}= −59 ± 6 cal/mol/*m*) was obtained by (8).

[g]From VPO data shown in Figure 2B. Calculation of μ_{23} per accessible surface area of anionic oxygens takes into account μ_{23} for K^+, aliphatic carbon and hydroxyl O reported by (8), as described in the text.

[h]Data from (33).

[i]From VPO data shown in Figure 2C.

Table 3

Average SASA of different RNA conformations[a]

Model	PO_2^-	ribose	base
Helix[b]			
Average xtal	69.3	77.3	30.3
A-form	70.8	76.4	30.5
5, 3′ terminus	74.8	128.1	81.9
single strand, A-form coordinates[c]			
average internal	68.1	77.2	74.7
Y nucleotide	66.9	77.0	61.5
R nucleotide	69.3	77.5	87.8
average terminal	74.8	128.1	133.2
single strand, extended conformation[d]			
	56.3	103.7	131.9

[a]SASA were derived using a probe radius of 1.4 Å and are in units of $Å^2$ per nucleotide. PO_2^- is the sum of P and anionic oxygen (OP1 and OP2) surfaces; P itself contributes <3.5 $Å^2$.

[b]Average SASA per helical nucleotide were taken either from RNA crystal structures (average xtal) or a helix generated from standard coordinates (A-form). The average of 5′ and 3′ terminal nucleotides was taken from the generated helix.

[c]Average SASA were calculated from a single-strand sequence with standard A-form helical coordinates, for the indicated nucleotide positions (internal or terminal) or type (R, purine or Y, pyrimidine).

[d]SASA were averaged from portions of RNA crystal structures in unstacked conformations.

Biochemistry. Author manuscript; available in PMC 2013 November 06.

Table 4

ΔSASA and calculated *m*-values for RNA unfolding[a]

RNA	Native			Unfolded			ΔSASA			K^+ or KCl	Total
	PO_2^-	ribose	base	PO_2^-	ribose	base	PO_2^-	ribose	base		ΔSASA or *m*-value
poly(A)											
A-form ss, Å^2				69.3	77.5	87.8				0.8 K^+, −0.2 Cl^-	234.6 Å^2
μ_{23}				−25.0	−9.3	−57.9				92.0	−0.2 cal/mol/^{m}
extended ss, Å^2				56.4	103.7	131.9				0.8 K^+, −0.2 Cl^-	
μ_{23}				−20.3	−12.4	−87.1				92.0	−27.8 cal/mol/*m*
Hairpin	842	1029	467								
A-form ss, Å^2				830	1028	1013	~0	~0	544		544 Å^2
m-value							0	0	−348	−7.4	−356 cal/mol/*m*
extended ss, Å^2				676	1244	1582	−166	215	1115		1164 Å^2
m-value							60	−26	−713	−7.4	−687 cal/mol/^{m}
Tar-tar*	989	1215	505								
all A-form ss, Å^2				1089	1235	1018	138	20.3	513		671 Å^2
m-value							−50	−2	−328	−27	−407 cal/mol/*m*
ss + unstacked, Å^2				1089	1438	1205	137	223	700		1061 Å^2
m-value							−50	−27	−448	−27	−552 cal/mol/*m*
A-riboswitch*	4703	4516	2234								
all A-form ss, Å^2				4751	5330	3161	48	813	926		1788 Å^2
m-value							−17	−98	−593	−47	−931 cal/mol/*m*
ss + unstacked, Å^2				4751	5533	3295	48	1017	1061		2126 Å^2
m-value							−17	−122	−679	−47	−1041 cal/mol/*m*

RNA	Native			Unfolded			ΔSASA			K^+ or KCl	Total
	PO_2^-	ribose	base	PO_2^-	ribose	base	PO_2^-	ribose	base		ΔSASA or *m*-value
TLR											
GAAA, Å^2	352	298	135	391	458	358	39	160	223		422 Å^2
receptor (1TLR), Å^2	758	591	340	722	879	438	−36	289	99		352 Å^2
m-value							−1	−54	−205	−50	−311 cal/mol/*m*
receptor all ss, Å^2				757	850	568	42	259	228		
m-value							−15	−50	−289	−50	−404 cal/mol/*m*
receptor all helix, Å^2				762	850	333	42	259	−7		
m-value							−15	−50	−140	−50	−256 cal/mol/*m*

[a]The following nucleotides were included in both the native and unfolded state calculations of SASA; nucleotides omitted from the calculations have the same conformation in each state:

hairpin: 6 base pair helix

tar-tar*: for each RNA, the 6 nt hairpin loop plus a single closing base pair.

A-riboswitch: 69 nucleotides, excluding 5′, 3′ terminal base pair. The adenine ligand is considered solvent inaccessible in the native state, and completely accessible in the unfolded state.

TLR: 6 nts of the GAAA tetraloop, 19-24; 11 nts of the receptor, 5-9, 34-39 (numbering as in Figure 1D).